ISSN 1330-3651 (Print), ISSN 1848-6339 (Online)
UDC/UDK 621.6.04-522.7:531.314

CHARACTERISTICS OF GAS-SOLID TWO-PHASE FLOW IN AXIAL AND SWIRLING FLOW PNEUMATIC CONVEYING

Liu Songyong, Gao Kuidong, Cui Xinxia, Yang Daolong, Liu Xiaohui

Original scientific paper
To improve the capacity and efficiency of pneumatic conveying systems, a swirling flow generator was developed to achieve swirling flow pneumatic conveying (SFPC) for particles. A numerical simulation of axial flow pneumatic conveying (AFPC) and swirling flow pneumatic conveying (SFPC) for particles was carried out using the Lagrange particle tracking method (LPTM), in which the interactions of the gas phase and solid phase were taken into account. The distributions of particle concentration and particle velocity were analysed. The results indicate that the distribution of particle concentration was improved by swirling flow and that of the particle velocity increased first and then decreased with swirling flow intensity; however, the particle velocity still increased by more than 40 % relative to the velocity observed in AFPC. Swirling flow exhibited the optimal behaviour when the swirling intensity was approximately 0,3. The swirling intensity decayed faster with greater axial gas velocity exponentially. The results of pressure loss experiments in AFPC and SFPC showed that there was an optimal gas velocity in AFPC that minimised the pressure loss. The optimal gas velocity increased with mass flow rate; the pressure loss in SFPC first increased and then decreased with swirling intensity. The maximum pressure loss in SFPC was larger than that in AFPC while the swirling intensity was 0,35; 0,376; 0,38 and the mass flow rate was 1,5 kg/s; 1,9 kg/s; 2,5 kg/s. The pressure loss in SFPC was lower than that in AFPC while swirling intensity was higher than a certain value.

Keywords: *gas-solid two-phase flow, Lagrange particle tracking, pneumatic conveying, swirling flow*

Karakteristike dvofaznog protoka plin-čvrsta tvar u pneumatskom prenošenju aksijalnim i vrtložnim protokom

Izvorni znanstveni članak
U svrhu povećanja kapaciteta i učinkovitosti pneumatskih sustava prenošenja razvijen je generator vrtložnog protoka za postizanje pneumatskog prenošenja čestica vrtložnim protokom (SFPC). Provedena je numerička simulacija pneumatskog prenošenja čestica aksijalnim protokom (AFPC) i pneumatskog prenošenja čestica vrtložnim protokom (SFPC) primjenom Lagrange metode praćenja čestica (LPTM) u kojoj su uzete u obzir interakcije plinske faze i čvrste faze. Analizirane su raspodjele koncentracije čestica i brzine čestica. Rezultati pokazuju da se vrtložnim protokom poboljšala raspodjela koncentracije čestica i da je najprije porasla a zatim se smanjila brzina čestica kod pojačanog vrtložnog protoka; ipak se brzina čestica povećala za više od 40 % u odnosu na brzinu u AFPC. Vrtložni je protok pokazao optimalno ponašanje kod intenziteta vrtloženja od približno 0,3. Intenzitet vrtloženja brže se smanjivao s eksponencijalno većom aksijalnom brzinom plina. Rezultati eksperimenata o gubitku tlaka u AFPC i SFPC pokazali su da postoji optimalna brzina plina u AFPC koja je minimalizirala gubitak tlaka. Optimalna se brzina plina povećavala s količinom protoka mase; gubitak tlaka u SFPC najprije je porastao a zatim se smanjio s pojačanjem vrtloženja. Maksimalni gubitak tlaka u SFPC bio je veći od onoga u AFPC dok je vrtložni intenzitet bio 0,35; 0,376; 0,38, a količina protoka mase 1,5 kg/s; 1,9 kg/s; 2,5 kg/s. Gubitak tlaka u SFPC bio je manji nego u AFPC dok je intenzitet vrtloženja bio veći od određene vrijednosti.

Ključne riječi: *dvofazni protok plin-čvrsta tvar, pneumatsko prenošenje, praćenje čestica po Lagrangeu, vrtložni protok*

1 Introduction

Pneumatic conveying is widely used in the petroleum, chemical, food, mining, ceramic and metal industries, among others [1]. There are two forms of pneumatic conveying: dilute and dense phase conveying [2]. This study focussed on the analysis of the dilute phase conveying of gangue particles. Herbreteau [3] studied the factors affecting energy consumption in horizontal pneumatic conveying and indicated that pneumatic conveying systems consumed large amounts of energy. Rinoshika [4] carried out an experimental study on pneumatic conveying in a horizontal pipeline with a dune model. The experimental results indicated that a lower conveying velocity and energy-saving conveying could be realised by installing a dune model in the conveying pipeline. Hui-Li and Tomita [5, 6] studied a swirling flow pneumatic conveying system by using a swirling flow generator, and their study results demonstrated that energy-saving conveying could be realised in low-velocity pneumatic conveying. However, the swirling flow generator could only be installed in the gas flow section, and its application was limited. According to Pan [7], blockage can easily occur in areas where gas flow is insufficient. Moller [8] invented the turbulence double-pipe system to overcome such blockage, but the secondary pipe was mounted in the conveying pipeline and occupied the space of the conveying pipeline.

In this study, a new swirling flow generator used in gas-solid two-phase flow experiments was devised to realise swirling flow pneumatic conveying. The gangue particle size used in the experiments was 10 ÷ 15 mm, and the experiments were designed to investigate dilute phase conveying in particular. A comparative analysis of the characteristics of gas-solid two-phase flow between axial and swirling flow pneumatic conveying was conducted, the results of which provide a reference for energy-saving conveying and improving the performance of pneumatic conveying systems.

2 Numerical model of gas-solid two-phase flow

There are two numerical methods used to evaluate pneumatic conveying: the gas-solid two-phase coupling method (GTCM) and the Lagrange particle tracking method (LPTM) [9]. Fokeer [10] compared the two methods and concluded that the LPTM was better suited for studying dilute phase pneumatic conveying. In the LPTM, the gas is treated as a continuum by solving the appropriate flow control equations, whereas the solid is treated by tracking a large number of solid particles. The gas and solid phases are not independent; in fact, particles

can exchange momentum and energy with the gas phase [11].

2.1 Control equations for gas phase

The control equations for the gas phase can be derived by assuming that the gas is incompressible and the gas-solid flow is steady. Gas flow is calculated based on the time-averaged Navier-Stokes equations in accordance with the $k-\varepsilon$ turbulence model [12].

Continuity equation for gas phase:

$$\frac{\partial}{\partial x_i}(\rho v_i) = 0 . \quad (1)$$

Momentum equation for gas phase:

$$\frac{\partial}{\partial x_j}(\rho v_i v_j) = -\frac{\partial p}{\partial x_i} + \frac{\partial \tau_{ij}}{\partial x_j} + \rho g_i , \quad (2)$$

where ρ is the gas density, v is the gas velocity, p is the gas pressure, τ_{ij} is the stress tensor of an infinitesimal body and g is the acceleration of gravity.

The turbulent kinetic energy k and the rate of turbulent dissipation ε are obtained from the transport Eqs. (3) and (4).

$$\frac{\partial}{\partial x_i}(\rho k u_i) = \frac{\partial}{\partial x_j}\left[(\mu + \frac{\mu_t}{\sigma_k})\frac{\partial k}{\partial x_j}\right] + G_k + G_b - \rho\varepsilon - Y_M + S_k \quad (3)$$

and

$$\frac{\partial}{\partial x_i}(\rho \varepsilon u_i) = \frac{\partial}{\partial x_j}\left[(\mu + \frac{\mu_t}{\sigma_\varepsilon})\frac{\partial \varepsilon}{\partial x_j}\right] + C_{1\varepsilon}\frac{\varepsilon}{k}(G_k + C_{3\varepsilon}G_b) - C_{2\varepsilon}\rho\frac{\varepsilon^2}{k} + S_\varepsilon , \quad (4)$$

where $C_{1\varepsilon}$, $C_{2\varepsilon}$, C_μ, σ_k and σ_ε are the model constants (the default values are as follows: $C_{1\varepsilon}$=1,44; $C_{2\varepsilon}$=1,92, C_μ=0,09; σ_k=1,0; σ_ε=1,3), μ_t is the turbulent viscosity, G_k is the generation of turbulence kinetic energy due to the mean velocity gradients, G_b is the generation of turbulence kinetic energy due to buoyancy, Y_M is the contribution of the fluctuating dilatation in compressible turbulence to the overall dissipation rate and S_k and S_ε are user-defined source terms [13].

2.2 Differential equation for solid phase

In accordance with Newton's second law, the differential equation for particle movement in a horizontal pipeline is as follows:

$$m_p \frac{dv_p}{dt} = F_d + F_g + F_x , \quad (5)$$

where m_p is the particle mass, v_p is the particle velocity, F_d is the particle drag force, F_g is the force of gravity acting on the particle and F_x represents other forces acting on the particle, including the Saffman lift force due to fluid shearing motion and the Magnus lift force due to particle rotation. Compared to the drag force and Saffman lift force, the Magnus lift force and other forces are small in magnitude and can be neglected [14].

Fluid resistance:

$$F_d = \frac{3}{4}\frac{\rho m_p}{\rho_p d_p} C_d (v - v_p)\left|v - v_p\right|, \quad (6)$$

where ρ_p is the particle density, d_p is the particle diameter and C_d is the drag coefficient.

The simulated and experimental particles were non-spherical, and thus, the correlation developed by Haider and Levenspiel [14], indicated by Eqs. (7) to Eq. (12), was adopted:

$$C_d = \frac{24}{Re_{sph}}(1 + b_1 Re_{sph}^{b2}) + \frac{b_3 Re_{sph}}{b_4 + Re_{sph}}, \quad (7)$$

and

$$b_1 = e^{2,3288-6,4581\varphi+2,4486\varphi^2}, \quad (8)$$

$$b_2 = 0,0964 + 0,5565\varphi, \quad (9)$$

$$b_3 = e^{4,905-13,8944\varphi+18,4222\varphi^2-10,2599\varphi^3}, \quad (10)$$

$$b_4 = e^{1,4681+12,2584\varphi-20,7322\varphi^2+15,8855\varphi^3}, \quad (11)$$

$$Re_{sph} = \frac{\rho d_p \left|u_p - u\right|}{\mu}, \quad (12)$$

where φ is the shape factor and d_p is the diameter of a sphere with the same volume as the actual particle [13].

The recovery factor of particle-wall collision was obtained by Forder's recovery factor equations [15]. The equations were established by the collision test of sand and alloy steel which included the normal recovery factor e_n and the tangential recovery factor e_r. The two factors are expressed by impact angle θ.

$$e_n = 0,988 - 0,78\theta + 0,19\theta^2 - 0,024\theta^3 + 0,027\theta^4, \quad (13)$$

$$e_r = 1 - 0,78\theta + 0,84\theta^2 - 0,021\theta^3 + 0,028\theta^4 - 0,022\theta^5. \quad (14)$$

This study was mainly concerned with determining the particle distribution with respect to particle concentration and particle velocity and pressure loss in axial and swirling flow pneumatic conveying by contrasting the effects of axial and swirling flow. The particle velocity distribution reflected the conveying capacity of pneumatic conveying. The particle distribution was determined by numerical simulation and the pressure loss by pneumatic conveying experiments.

3 Simulations of particles pneumatic conveying in axial and swirling flow

The FLUENT software program was used to simulate axial and swirling flow pneumatic conveying based on a mathematical model. For axial flow, the length of the axial flow pipe was set to 10 m and the diameter to 70 mm. The meshes of the axial flow pipe shown in Fig. 1a were composed of hexahedral elements. For swirling

flow, a swirling flow generator was added in the middle of the axial flow pipe, which was called the swirling flow pipe. The length of the swirling flow pipe was set to 10 m. The structure of the swirling flow pipe is shown in Fig. 1b. The swirling flow generator was composed of two assistant pipes and one main pipe. The assistant pipes were positioned around the main pipe, and the space angle between the assistant pipes and the main pipe was α. The assistant pipes did not occupy space in the pipelines and could be installed in the conveying pipeline. The diameter of the main pipe was 70 mm, and that of the assistant pipe was 20 mm. The meshes of the swirling flow pipe were composed of hexahedral elements. The meshes were refined in the swirling flow generator.

For the axial and swirling flow, the x-axis direction was the pipeline axis and the y-axis direction was the vertical direction. The acceleration of gravity was along the $-y$ direction.

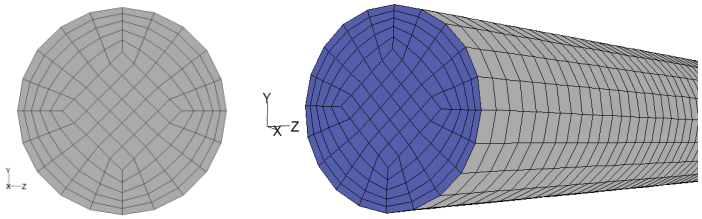

(a) Axial conveying pipes

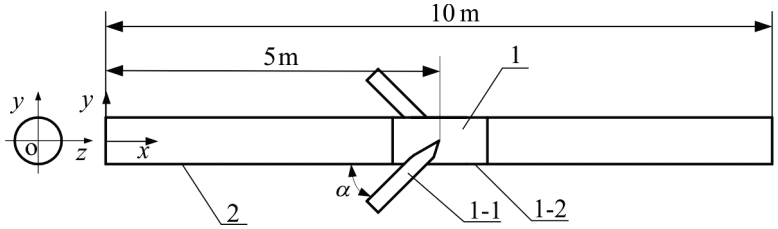

1 - Swirling flow generator, 2 - Axial flow pipe, 1-1 - Swirling flow assistant pipe, 1-2 - Swirling flow main pipe

(b) Structure of swirling flow pipe

Figure 1 Physical model of swirling flow pipe

Table 1 Boundary condition

Boundary	Type	Parameter
Axial flow pipe inlet	Velocity inlet	40 m/s
Swirling flow pipe inlet	Velocity inlet	20 m/s, 25 m/s, 30 m/s
Swirling flow Assistant pipe inlet	Velocity inlet	122,5 m/s, 91,25 m/s, 61,25 m/s
Axial flow pipe outlet	Pressure outlet	0,101325 MPa (1 atm)
Swirling flow pipe outlet	Pressure outlet	0,101325 MPa (1 atm)
Wall	No slip	Roughness=0,05 mm

Table 2 Parameters of particle injection

Parameters	Value
Particle density (ρ_p)	2800 kg/m^3
Particle size (d_p)	10 mm
Particle shape	Sphere
Particle shape factor (k)	1
Particle velocity (v_p)	0 m/s
Particle mass flow rate (f_p)	1,5 kg/s

Combining with the pneumatic conveying experiments, the boundary conditions were set as shown in Tab. 1. The gas velocity of the axial flow pipe inlet was 40 m/s, and the gas mass flow rate was 0,188 kg/s. The gas velocities at the swirling flow pipe inlet were 20 m/s, 25 m/s and 30 m/s. The gas velocities at the swirling flow assistant pipe inlet were 122,5 m/s, 91,25 m/s and 61,25 m/s. The collision recovery factor of the pipe wall was calculated using Eq. (13) and Eq. (14). The roughness of the wall was 0,05 mm. The spherical particles were injected uniformly from the axial flow pipe inlet and swirling flow pipe inlet; the parameters of the injected particles are shown in Tab. 2. The transport medium was air, which was incompressible because the gas velocity was small (Ma < 0,2). The gas density was 1,225 kg/s, and the dynamic viscosity was $1{,}8\times10^{-5}$ m^2/s.

The strength of the swirling flow in the pneumatic conveying was measured by the swirling intensity [5, 16], which was calculated using Eq. (15).

$$S=\frac{\int \rho u\sqrt{v^2+w^2}\sqrt{y^2+z^2}\,\mathrm{d}A}{R\int \rho u^2\,\mathrm{d}A}, \tag{15}$$

where u, v and w denote the gas velocity along the x-, y- and z-directions, respectively; y and z are the values of y- and z-coordinates, and R is the pipe radius.

The surface integral function was used to calculate the swirling number in the FLUENT software program. For the swirling flow pipe, the different gas velocities at the pipe inlet and assistant pipe inlet combined to produce different swirling intensities. The method of gas-solid two-phase coupling was used to analyse the simulation result and the particle distribution in pneumatic conveying.

4 Result analysis of numerical simulation

4.1 Particles tracking

Particle tracking was performed by the method of gas-solid tow-phase coupling, as shown in Fig. 2. The pipe was scaled along the x-axis by a scale factor 0,05. Parts of the particle trajectories are shown in Fig. 2.

As shown in Fig. 2a, the particles in axial flow mainly subsided to the bottom of the pipelines, and the

rebound height of particle-wall collisions decreased gradually. As shown in Fig. 2b, the particle trajectories in swirling flow were different from those in axial flow at S=0,34 and v_z=20 m/s. When the particles entered the swirling flow generator (the middle position x=5 m), the rebound height of particle-wall collisions increased again and the particle trajectory presented spiralling motion. This result indicated that the swirling flow caused the particles to subside to the bottom of the pipelines and re-enter flow, but the spiralling motion of the particles decreased gradually with the gas-solid flow downstream. Compared with that shown in Fig. 2b, the effect of the swirling flow shown in Fig. 2c was reduced due to the high particle velocity. As indicated in Fig. 2d, the swirling intensity increased to 0,55 and the particle trajectory presented spiralling motion, similar to that shown in Fig. 2b, but the spiral motion of particles shown in Fig. 2b was more intense than that shown in Fig. 2d.

The particle trajectory in swirling flow showed "jumps" and was different from that in axial flow in the first half of the swirling flow pipe (x<5 m). This behaviour was due to the secondary flow produced with the decrease in gas velocity. The secondary flow, which altered the particle trajectories, is shown in Fig. 3 and features two swirling flows. The maximum flow velocity was approximately 13 % of the axial flow velocity.

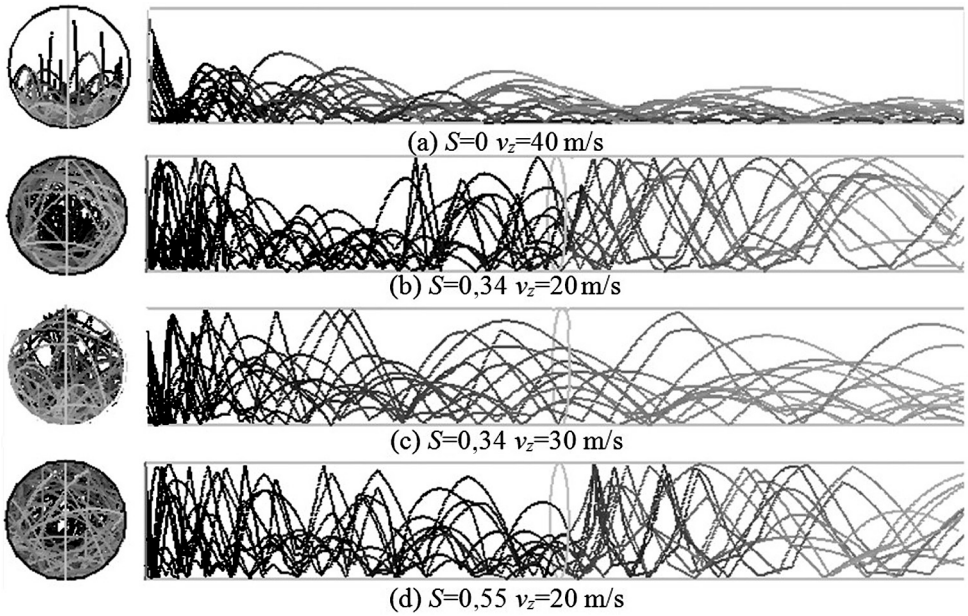

Figure 2 Particle trajectory

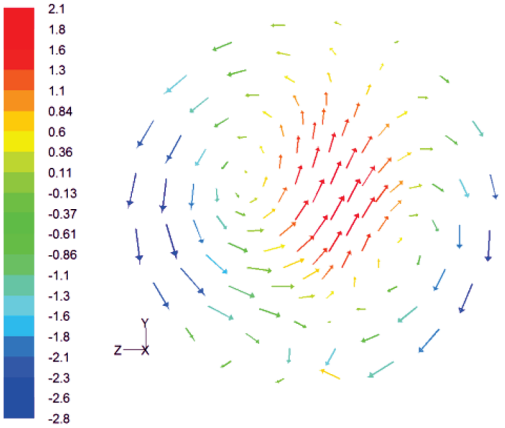

Figure 3 Secondary flow

4.2 Particle concentration distribution

The particle distributions in the axial and swirling flow pipes are shown in Fig. 4. In the axial flow pipe, particles were mainly distributed at the bottom of the pipeline due to gravity, and the particle distribution was symmetric about z=0. In the swirling flow pipe, the particles distributed uniformly within the section and filled the entire pipeline section. However, in the swirling flow, especially when the swirling intensity was high, the particles tended to distribute along the wall, and there were fewer particles in the middle of the pipe. Thus, swirling flow could effectively overcome the effect of gravity.

The particle distribution was measured qualitatively as shown in Fig. 4. A statistical method was used to measure the effect of the particle distribution on swirling flow quantitatively. The effect of gravity was taken into account when analysing the particle distribution in different sections along the vertical direction. The section was divided into 14 regions in the vertical direction, each with a height of 5 mm. The number of particles and the particle velocity in each region were calculated using Eq. (16) to Eq. (18).

$$v_{\mathrm{p}} = \frac{1}{N_i}\sum_{j=1}^{N_i} v_{\mathrm{p}ij}, \tag{16}$$

$$v_{\mathrm{p\,av}} = \frac{1}{N}\sum_{i=1}^{7}\sum_{j=1}^{N_i} v_{\mathrm{p}ij}, \tag{17}$$

$$\frac{\rho_s}{\rho_{s0}} = \frac{A}{a_i}\frac{N_i}{N} \tag{18}$$

where N_i is the number of particles in area i, $v_{\mathrm{p}ij}$ is the velocity of particle j in area i, N is the total number of particles, A is the area of section, a_i is the area of area i, v_{p}

is the local average particle velocity, ρ_s is the local average particle concentration, $v_{\text{p av}}$ is the global average particle velocity and ρ_{s0} is the global average particle concentration [5, 6].

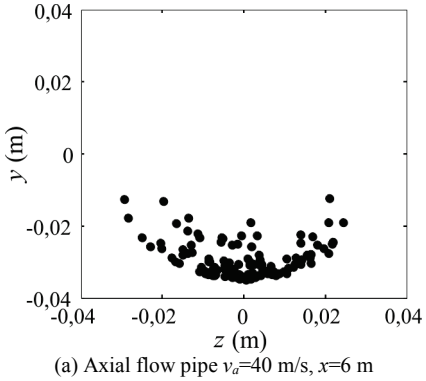

(a) Axial flow pipe v_a=40 m/s, x=6 m

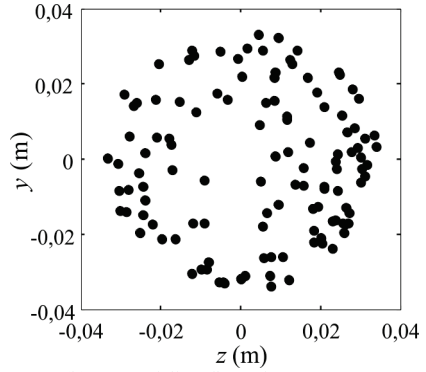

(b) 45° Swirling flow pipe S=0,545

Figure 4 Particle distributions in axial flow pipe and swirling flow pipe

The particle concentration distribution at different swirling intensities is shown in Fig. 5. The value S=0 indicates axial flow. As shown in Fig. 5a, the velocity at the swirling flow pipe inlet was 30 m/s (v_z=30 m/s) and the velocity at the swirling flow assistant pipe inlet was 61,25 m/s (v_f=61,25 m/s). Fig. 5a indicates that the swirling flow improved the particle distribution, with particles moving to the top of the pipeline. The particle distribution improved gradually with swirling intensity. A comparison of Fig. 5a and Fig. 5b reveals that the gas velocity decreased to 20 m/s at the swirling flow pipe inlet and increased to 122,5 m/s at the swirling flow assistant pipe inlet. The swirling intensity increased, but the total gas consumption remained unchanged. The particle distribution shown in Fig. 5b is different from that shown in Fig. 5a. There were fewer particles in the middle of pipeline, and the number of particles increased gradually close to the wall. As shown in Fig. 5c, the swirling intensity was 0,34 (S=0,34) and the gas velocities were different. The minimum particle concentration occurred at y=0. Due to the velocity at the swirling flow pipe inlet, the particle distribution was deflected in the counter clockwise direction and the particle concentration increased at the bottom of the pipeline. This behaviour was observed because the axial velocity of the particles entering the swirling flow increased with the velocity at the swirling flow pipe inlet, and the spiral motion of the particles was also enhanced.

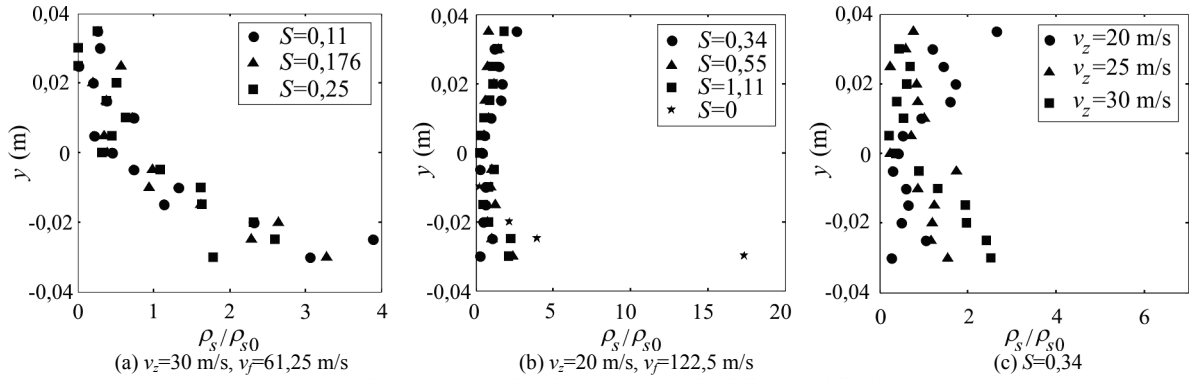

(a) v_z=30 m/s, v_f=61,25 m/s (b) v_z=20 m/s, v_f=122,5 m/s (c) S=0,34

Figure 5 Particle concentration distribution at x=6 m for different swirling intensities

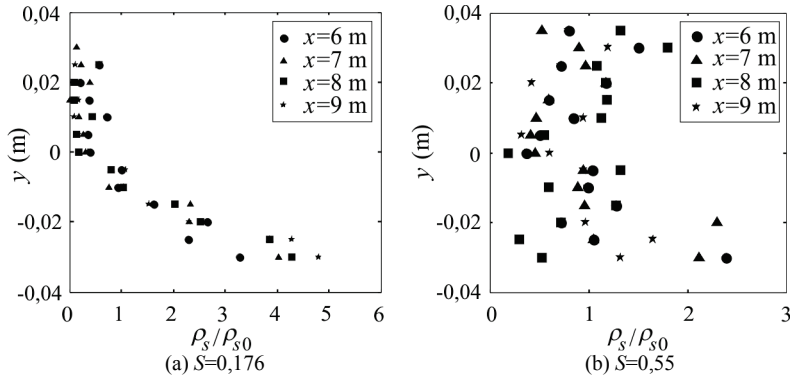

(a) S=0,176 (b) S=0,55

Figure 6 Particle concentration distribution at S=0,176 and S=0,55 along different cross-sections

The particle distributions along different cross-section are shown in Fig. 6. As shown in Fig. 6a, the number of particles that subsided to the bottom of the pipeline increased with particle concentration, which meant that the swirling intensity was decaying. Fig. 6b shows that the particle distribution along different cross-

sections was similar to that shown in Fig. 5b, but there are no signs that the swirling intensity decayed, demonstrating that the greater the swirling intensity was, the longer the effective distance of swirling flow was.

4.3 Swirling flow

The swirling flow could weaken the particle subsidence. The gas velocities in axial and swirling flow at x=6 m are shown in Fig. 7. In axial flow pneumatic conveying, gas flow occurred mainly at the top of the pipe due to the subsidence of particles to the bottom of the pipeline. In swirling flow pneumatic conveying, the gas velocity was symmetric about the centre of the axis. According to Fig. 6a, the swirling intensity decayed with particle conveying. The exponential decay of the swirling intensity is shown in Fig. 8, where l is the distance from the swirling assistant pipe inlet. The decay of the swirling intensity is expressed by Eq. (19).

$$\begin{cases} S(l) = 0{,}87\mathrm{e}^{-10{,}8l} + 0{,}24\mathrm{e}^{-1{,}65l} \\ S(l) = 0{,}27\mathrm{e}^{-4{,}4l} + 0{,}08\mathrm{e}^{-0{,}74l} \\ S(l) = 0{,}22\mathrm{e}^{-16{,}9l} + 0{,}13\mathrm{e}^{-1{,}4l} \end{cases}. \quad (19)$$

In the same swirling intensity, the swirling intensity decreased to 0,039 when the velocity of swirling flow pipe inlet was 25 m/s after a distance of 1 m, while when the velocity was 30 m/s, the intensity decreased to 0,032, which proved that the larger the velocity of swirling flow pipe inlet was, the faster the decay of swirling intensity was.

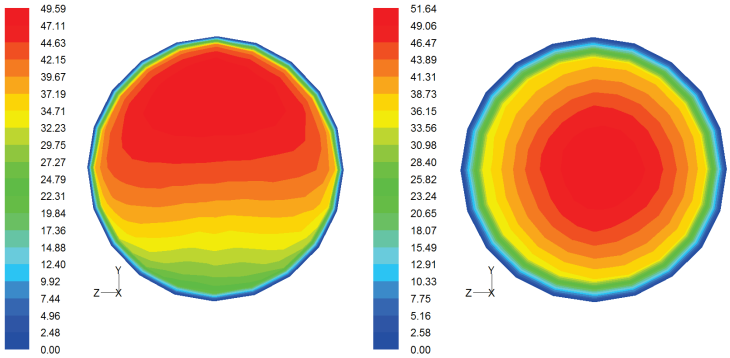

(a) Axial flow (b) Swirling flow

Figure 7 Gas velocity in x=6 m

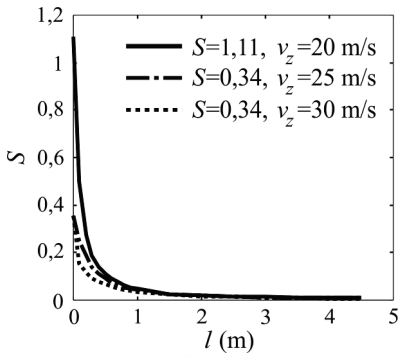

Figure 8 Swirling intensity decay

4.4 Particle velocity distribution

Compared with axial flow pneumatic conveying, swirling flow conveying dispersed the particle distribution and altered the interaction between the particles and gas. The distribution of the particle velocity at different swirling intensities is shown in Fig. 9, where S=0 indicates axial flow. The standard deviation of the particle velocity in each region is also shown in Fig. 9. In Fig. 9a and Fig. 9b, the distribution of the particle velocity is relatively uniform in swirling flow pneumatic conveying. The particle velocity in the central area is higher than that in other areas when S=0,176 ÷ 0,55. In Fig. 7b, the distribution of the gas velocity could explain the distribution of the particle velocity. The distribution of the particle velocity at S=0,11 and that at S=1,11 are different because the swirling intensity was either too low or too high. Fig. 9a shows that the particle velocity increased and the standard deviation decreased with the increase in swirling intensity, which improved the consistency of the particles. The effect was due to the fact that the axial fluid drag force acting on the particles increased and the effects of gravity and turbulent diffusion weakened. Fig. 7b shows that the particle velocity decreased and the standard deviation increased with swirling intensity due to the large swirling intensity and the severe particle-wall collisions. Therefore, there was an optimal swirling intensity at which the particle velocity was maximised, namely, S=0,25 ÷ 0,34.

The particle velocity distribution in different sections at S=0,176 and S=0,55 is shown in Fig. 10. Fig. 10a shows that the particle velocity decreased at the bottom of pipeline, whereas it increased at the top of the pipeline. Combined with the results presented Fig. 6a, it was determined that the particles tended to subside at the bottom of the pipeline. Fig. 10b shows that the particle velocity did not tend to decrease due to the swirling motion of the particles, which altered the distribution of the particle velocity.

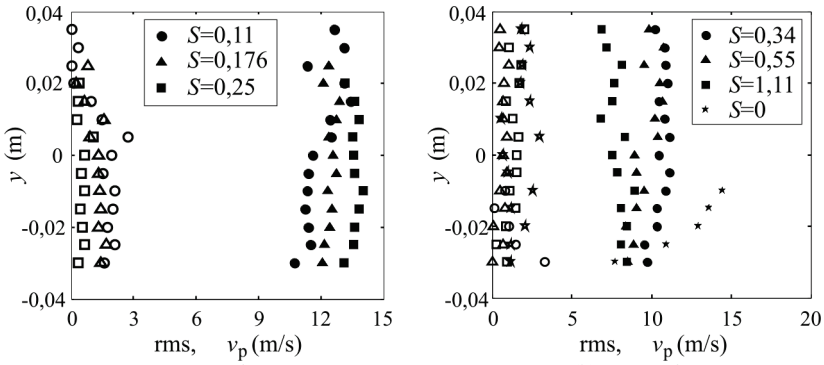

(a) v_z=30 m/s (b) v_z=20 m/s

Figure 9 Particle velocity distributions at x=6 m for different swirling intensities

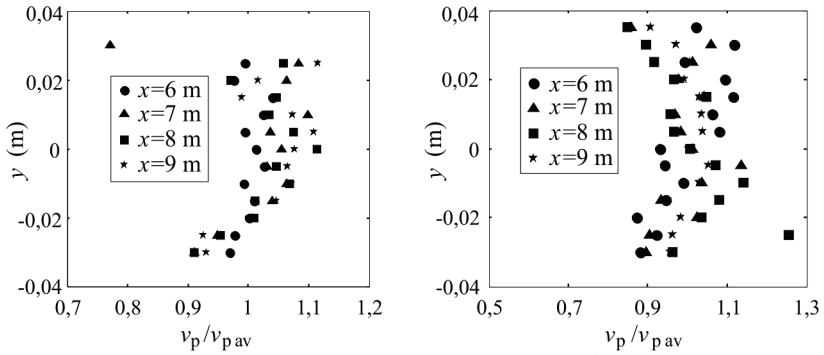

(a) S=0,176 (b) S=0,55

Figure 10 Particle velocity distributions in different cross-sections

The axial change in particle velocity in the pipeline is shown in Fig. 11, where S=0 indicates axial flow. The change in particle velocity showed the same tendency, and the particles were in accelerated motion at x<5 m. The higher the velocity at the swirling flow pipe inlet was, the greater the acceleration of the particles became. The particles accelerated again at x>5 m, and the particle velocity in swirling flow was higher than that in axial flow. At the same swirling intensity, the higher the velocity at the swirling flow pipe inlet was, the higher the velocity of the particles became. The difference was mainly caused by the different acceleration of the particles in the first half pipeline. At the same velocity at swirling flow pipe inlet, the particle at S=0,34 was faster than that at S=0,55 due to the high swirling intensity (S=0,74) and the severe particle-wall collisions, which made the particles accelerate more slowly.

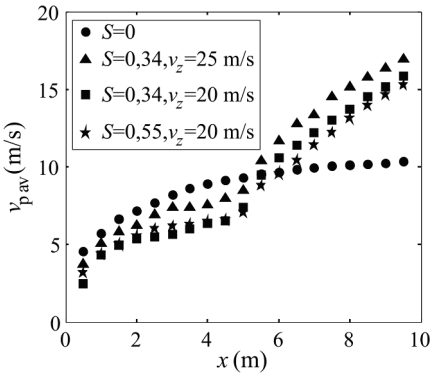

Figure 11 Axial change in particle velocity in pipe

The relationship between particle velocity and swirling intensity at x=10 m is shown in Fig. 12. The vertical ordinate was the specific value between the particle velocity in spiraling flow and that in axial flow. The particle velocity in swirling flow was higher than that in axial flow. The specific value increased firstly then decreased with swirling intensity. The maximum value was acquired in S=0,25 ÷ 0,35 and the maximum value was 1,74. That meant in the same gas consumption, the particle velocity in swirling flow was 74 % higher than that in axial flow, which reduced the particle subsidence and the risk of blockage effectively and improved the transmission capacity of pneumatic conveying.

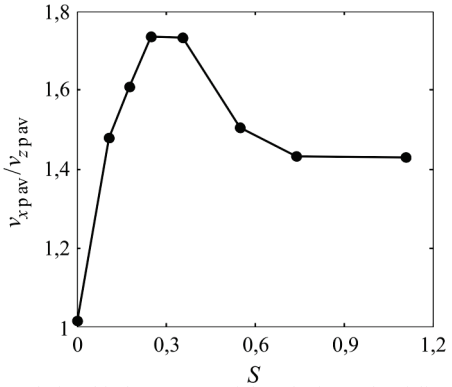

Figure 12 Relationship between particle velocity and swirling intensity

5 Pressure losses

The analysis of particle distribution and velocity showed that the swirling flow generator could improve both properties and alleviate particle subsidence. The gas flow in AFPC was different from that in SFPC. The change in pressure along the pipe axis in AFPC and SFPC at S=0,55 is shown in Fig. 13.

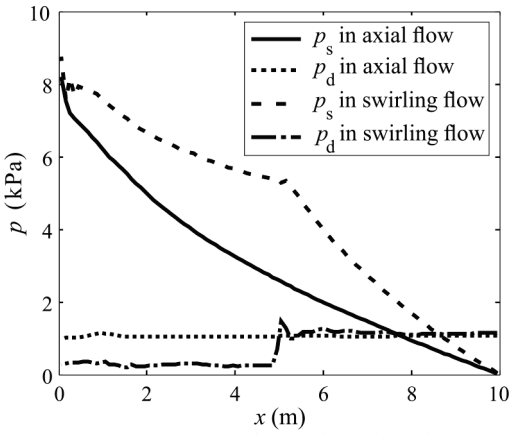

Figure 13 Pressure change along pipe axis

The pressure loss was embodied by the static pressure, whereas the dynamic pressure essentially remained unchanged along the pipe axis. The pressure in SFPC was similar to that in AFPC. At the entrance of swirling flow pipe (x=5 m), due to the swirling flow, the static pressure and dynamic pressure increased appreciably. In initial segment of the pipe (x<0,25 m), the pressure loss was significantly higher than that at other positions because the particles were in the acceleration stage. According to the above analysis, the pressure loss was embodied by the static pressure loss.

5.1 Particle pneumatic conveying experiments

The particle pneumatic conveying experiments were carried out using pneumatic conveying equipment and a test system, which are shown in Fig. 14.

The pneumatic conveying equipment included a hopper, rotary feeder, gas source, control valve, injector, conveying pipeline and container. The rated speed of the feeder was 24 r/min. The feeding of particles was controlled by the frequency converter. The conveying pipelines were composed of 3 m seamless tubes measured 70 mm in diameter and 0,05 mm in roughness, and the total length was 22 m. The rapid joint flange was used to connect and seal the pipeline, which was equipped by the swirling flow generator and conveniently switched axial flow pneumatic conveying to swirling flow pneumatic conveying.

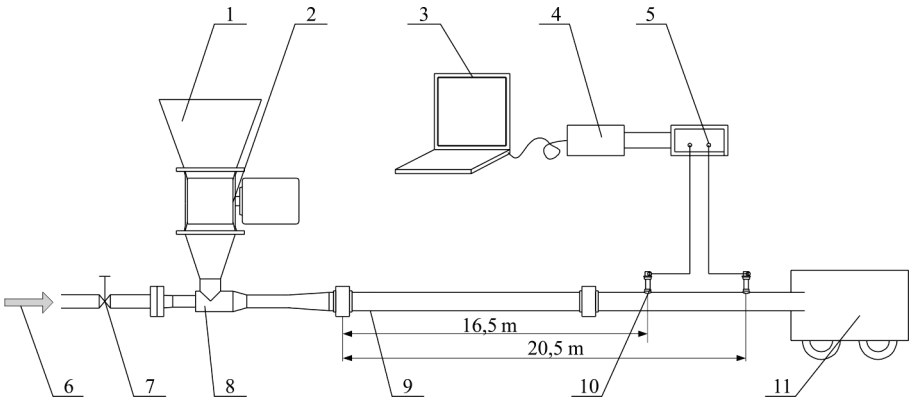

1 - Hopper, 2 - Rotary feeder, 3 - Computer, 4 - Data acquisition instrument, 5 - Signal amplifier, 6 - Gas source, 7 - Control valve, 8 - Injector, 9 - Conveying pipeline, 10 - Pressure transducer, 11 - Container

Figure 14 Pneumatic conveying test bench

The test system included pressure transducers, a signal amplifier, a data acquisition instrument and a computer. The pressure transducers were HSTL 20 transducers with a sensitivity of 3,33 V/MPa and detection range of 0 to 1,5 MPa. The pressure transducers were installed along the pipeline 4 m away from each other. The pressure loss was obtained by processing the signal obtained from the pressure transducers. The density of particles in the experiments was 2800 kg/m^3, and the packing density was 1024 kg/m^3. The diameter of the gangue particles was 10 ÷ 15 mm considered as polyhedron, and the particle mass flow rates were 1,5 kg/s; 1,9 kg/s and 2,4 kg/s. The gas velocity was set by a pilot tube and control valve.

5.2 Pressure loss of axial flow pneumatic conveying

The experiments concerning the measurement of particle and gas velocities at different mass flow rates were performed to determine the pressure loss in AFPC; the results are shown in Fig. 15.

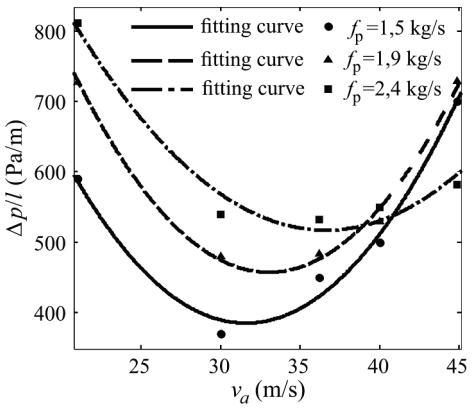

Figure 15 Pressure loss of axial flow pneumatic conveying

The particle mass flow rates were 1,5 kg/s; 1,9 kg/s and 2,4 kg/s. The results obtained for the three flow rates showed the same tendency: the pressure loss in AFPC decreased first and then increased with gas velocity when the gas velocity ranged from 20 to 45 m/s, which meant that there was an optimal gas velocity in AFPC that

minimised the pressure loss. The optimal gas velocity increased with particle mass flow rate. The optimal gas velocities at f_p=1,5; 1,9 and a mass flow rate of 2,4 kg/s were 31,6; 33,0 and 36,6 m/s. In actual applications, pneumatic conveying could be optimised by reducing the energy consumption at the optimal velocity.

5.3 Pressure loss of swirling flow pneumatic conveying

To compare the pressure loss in AFPC and that in SFPC, SFPC experiments were conducted at three different mass flow rates. Swirling flow was generated by a swirling flow generator. The gas flow rates in the swirling flow pipe and assistant pipe were controlled by a control valve to obtain different swirling intensities. The gas consumption in axial flow pipe equaled to that in swirling flow pipe, which could measure pressure loss comparably in AFPC and SFPC. In addition, the pressure transducers were arranged after the swirling flow generator.

The pressure loss per unit length is shown in Fig. 16. When the gas consumption was 0,188 kg/s, the results obtained for the three groups of experiments showed the same tendency. The pressure loss in SFPC increased first and then decreased with swirling intensity in the range of 0 to 0,8. The pressure loss under the different particle mass flow rates of 1,5; 1,9 and 2,4 kg/s reached the maximum level at the maximum swirling intensities (S_{max}) of 0,35; 0,376 and 0,38 respectively. The maximum swirling intensity increased with particle mass flow rate. The maximum pressure losses were 62 %, 59,7 % and 75 %, higher than those in AFPC.

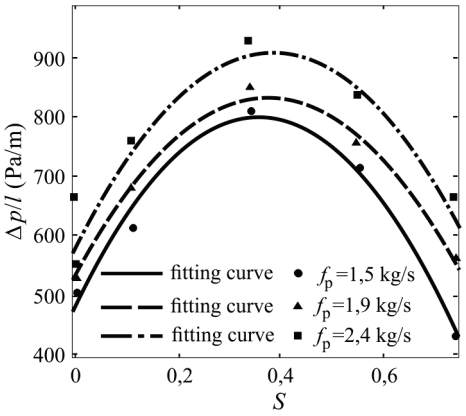

Figure 16 Relationship between swirling flow pressure loss and swirling intensity

Comparing the aforementioned results with those presented in Fig. 12 reveals that the increase in particle velocity occurred at the expense of an increase in pressure loss. When $S<S_{max}$, the pressure loss in SFPC was higher than that in AFPC, and the difference increased gradually. When $S>S_{max}$, the pressure loss in SFPC was still higher than that in AFPC, but the difference decreased gradually. The pressure loss was lower than that in AFPC when the particle mass ratio was 1,5 kg/s and the swirling intensity was 0,74, whereas the particle velocity in SFPC was 40 % higher than that in AFPC, which indicated that swirling flow could improve the gas flow energy consumption.

6 Conclusions

The characteristics of gas-solid two-phase flow were analysed comparatively between axial and swirling flow pneumatic conveying.

Particles were mainly distributed at the bottom of the pipeline in AFPC, whereas the particle distribution was improved and more uniform in SFPC. However, the swirling flow decayed faster with greater axial gas velocity exponentially. The particle velocity increased firstly and then decreased with swirling intensity. The particle velocity was improved by more than 40 % in SFPC compared with that in AFPC, and SFPC was optimised at a swirling intensity of approximately 0,3.

The results of pressure loss experiments in AFPC and SFPC showed that there was an optimal gas velocity in AFPC that minimised the pressure loss. The optimal gas velocity increased with particle mass flow rate. The pressure loss in SFPC increased first and then decreased with swirling intensity. The pressure loss was greater than that in AFPC, and as the swirling intensity increased further, the pressure loss in SFPC became lower than that in AFPC.

Acknowledgements

The authors gratefully acknowledge the National High Technology Research and Development Program of China (Grant No.2012AA062100), the National Natural Science Foundation of China (51375478).

7 References

[1] Xie Zhuo, Li; Li, Ming; Zhang, Zheng. Numerical Simulation of Horizontal Pneumatic Conveying. // Journal of Chemical Engineering of Chinese Universities. 20, (2006), pp. 331-337.
[2] Mills, D. Pneumatic Conveying Design Guide, Butterworth-Heinemann Ltd. Linacre House, London, 2004.
[3] Herbreteau, C.; Bouard, R. Experimental study of parameters which influence the energy minimum in horizontal gas-solid conveying. // Powder Technology. 112, (2000), pp. 213-220.
[4] Rinoshika, A.; Suzuki, M. An experimental study of energy-saving pneumatic conveying system in a horizontal pipeline with dune model. // Powder Technology. 198, (2010), pp. 49-55.
[5] Li, H.; Tomita, Y. Particle velocity and concentration characteristics in a horizontal dilute swirling flow pneumatic conveying. // Powder Technology. 107, (2000), pp. 144-152.
[6] Li, H.; Tomita, Y. Characterization of pressure fluctuation in swirling gas-solid two-phase flow in a horizontal pipe. // Advanced Powder Technology. 12, (2001), pp. 169-185.
[7] Pan, R. Material properties and flow modes in pneumatic conveying. // Powder Technology. 104, (1999), pp. 157-163.
[8] Levy, A.; Kalman, H. Handbook of Conveying and Handling of Particulate Solids, Elsevier Science B V, 2001.
[9] Kuang, S. B. Computational Study of Pneumatic Conveying by Discrete Element Model, PhD Dissertation, Shenyang: Northeastern University, 2009.
[10] Fokeer, S.; Kingman, S.; Lowndes, I. et al. Characterisation of the cross sectional particle concentration distribution in

horizontal dilute flow conveying - a review. // Chemical Engineering and Processing. 43, (2004), pp. 677-691.
[11] Zhou, L. X. Theory and numerical modeling of turbulent gas-particle flows and combustion, Science Press, Beijing, 1994.
[12] Huber, N.; Sommerfeld, M. Modeling and numerical calculation of dilute-phase pneumatic conveying in pipe systems. // Powder Technology. 99, (1998), pp. 90-101.
[13] ANSYS FLUENT 12.0 Theory Guide, ANSYS, Inc, United States, 2009.
[14] Lun, C. K. K.; Liu, H. S. Numerical Simulation of Dilute Turbulent Gas-Solid Flows in Horizontal Channels. // International Journal of Multiphase Flow. 23, 3(1997), pp. 575-605.
[15] Forder, A.; Thew, M.; Harrison, D. A numerical investigation of solid particle erosion experienced within oilfield control valves. //Wear. 216, (1998), pp. 184-193.
[16] Zhou, L. X.; Li, Y.; Chen, T. et al. Studies on the effect of swirl numbers on strongly swirling turbulent gas-particle flows using a phase-Doppler particle anemometer. // Powder Technology. 112, (2000), pp. 79-76.

Authors' addresses

Liu Songyong, Dr. *(corresponding author)*
School of Mechanical and Electrical Engineering,
China University of Mining and Technology
Xuzhou 221116, Jiangsu Province, China
E-mail: luck_honey@163.com

Gao Kuidong, Dr.
School of Mechanical and Electrical Engineering,
China University of Mining and Technology
Xuzhou 221116, Jiangsu Province, China
E-mail: gaokuidong22@163.com

Cui Xinxia, Dr.
School of Mechanical and Electrical Engineering,
China University of Mining and Technology
Xuzhou 221116, Jiangsu Province, China
E-mail: 17301421@qq.com

Yang Daolong, Dr.
School of Mechanical and Electrical Engineering,
China University of Mining and Technology
Xuzhou 221116, Jiangsu Province, China
E-mail: 349358486@qq.com

Liu Xiaohui, Dr.
School of Mechanical and Electrical Engineering,
China University of Mining and Technology
Xuzhou 221116, Jiangsu Province, China
E-mail: 823884259@qq.com